ISSN: 2447-3359

REVISTA DE GEOCIÊNCIAS DO NORDESTE

Northeast Geosciences Journal

v. 8, nº 1 (2022)

https://doi.org/10.21680/2447-3359.2022v8n1ID25675

Extraction of planimetric cartographic information by direct linear transformation with singular image obtained by remotely piloted aircraft

Extração de informações cartográficas planimétricas pela transformação linear direta com emprego de imagem obtida por aeronave remotamente pilotada

Jorge Felipe Euriques[1]; Edson Aparecido Mitishita[2]; Vinicius Gustavo Razoto[3]; Claudia Pereira Krueger[4]; Luís Augusto Koenig Veiga[5]

[1] Federal University of Paraná (UFPR), Curitiba/PR, Brasil. Email: jorge.euriques@ufpr.br
ORCID: https://orcid.org/0000-0001-9234-7551

[2] Federal University of Paraná (UFPR), Curitiba/PR, Brasil. Email: mitishita@ufpr.br
ORCID: https://orcid.org/0000-0003-1717-7657

[3] Federal University of Paraná (UFPR), Curitiba/PR, Brasil. Email: vrazoto@gmail.com
ORCID: https://orcid.org/0000-0002-3566-980X

[4] Federal University of Paraná (UFPR), Curitiba/PR, Brasil. Email: ckrueger@ufpr.br
ORCID: https://orcid.org/0000-0002-4839-131

[5] Federal University of Paraná (UFPR), Curitiba/PR, Brasil. Email: kngveiga@ufpr.br
ORCID: https://orcid.org/0000-0003-4026-5372

Abstract: Traditionally in Photogrammetry, the extraction of three-dimensional cartographic data involves the use of two images at least. With a singular image it is possible to obtain only planimetric information, however, external altimetry data is necessary for the execution of the process. The modeling of these informations is done rigorously by the Collinearity Equations (CLN) which assumption the use of camera calibration parameters and the treatment of systematic errors. Alternatively, generalized transformations such as Direct Linear Transform (DLT) can be used, simplifying the process. An investigation was developed aiming to verify the performance of the DLT and CLN models in extracting cartographic information using a single image. For this, an algorithm was implemented in Matlab. The image was obtained by a low-cost camera attached to a remotely piloted aircraft. Maximum discrepancy values around 0.80 m were obtained for planimetric values for both models. The RMSE for planimetric discrepancies was 0.53 m by CLN, and 0.56 m by DLT. The Cartographic Accuracy Standard for Digital Cartographic Products (PEC-PCD) was evaluated classifying in Class A by CLN and B by DLT, in the scale 1: 10000. DLT showed 90% efficiency in relation to rigorous formulation and operational advantages, in addition to not requiring camera parameters, which increases the possibility of using low-cost equipment.

Keywords: RPA; DLT; Collinearity Equations

Resumo: Tradicionalmente na Fotogrametria a extração de informações cartográficas tridimensionais envolve o uso de no mínimo duas imagens. O uso uma imagem pode-se obter apenas informações planimétricas, porém, dados de altimetria externos são necessários. A modelagem destas informações pode ser feita rigorosamente através das Equações de Colinearidade (CLN), que requer o uso de parâmetros de calibração da câmera e tratamento dos erros sistemáticos. Alternativamente, transformações generalizadas como a Direct Linear Transform (DLT) podem ser usadas. Neste trabalho apresenta-se um estudo que avaliou o desempenho da DLT frente às CLN na extração de informações cartográficas com o uso de uma imagem obtida por câmera de baixo custo acoplada a uma aeronave remotamente pilotada. Para isto um algoritmo foi implementado em Matlab. Obtiveram-se valores máximos de discrepância planimétrica em torno de 0,80 m para ambas as modelagens. O RMSE das discrepâncias planimétricas foi de 0,53 m pelas CLN e 0,56 m pela DLT. Avaliou-se o Padrão de Exatidão Cartográfica para Produtos Cartográficos Digitais (PEC-PCD), enquadrando-se na Classe A pelas CLN e B pela DLT, na escala 1:10000. A DLT apresentou eficiência de 90% na obtenção de coordenadas em relação às CLN, tendo vantagens operacionais, além de não requerer parâmetros da câmera, o que amplia a possibilidade do emprego de equipamentos de baixo custo.

Palavras-chave: RPA; DLT; Equações de Colinearidade.

Received: 21/06/2021; Accepted: 12/07/2021; Published: 14/06/2022.

1. Introduction

Since the beginnings of civilization, objects and cartographic features representations always have been necessary, such as property boundary delimitations, positioning, or navigation (GHILANI; WOLF, 2008). As time went by, geospatial information became a starting point for many applications, because of its univocal positional referential on the surface of Earth (AWANGE; KYALO KIEMA, 2013). These applications require different precision levels, depending on the combination of methods, techniques, and equipment available. This combination should be chosen to obtain an optimized solution, considering the best benefit-cost. Among the data acquisition methods, Photogrammetry is the science that allows physical surface cartographic information (object space) from images (image space), without direct physical contact with the object or target of interest (COELHO; BRITO, 2007).

The information extraction in tridimensional photogrammetric traditionally takes place through restitution using at least a pair of images that contains two views of a scene side by side (stereo-pair image). In these cases, stereoscopic vision allows image displacement correction caused by the object's height variation in the central projection (ABREU; ANTUNES, 2017). Nowadays processing strategies comes from computational vision, for example, SIFT (Scale Invariant Feature Transform) and SFM (Structure From Motion), which turns three-dimensional mapping feasible, even using a block of monocular images taken from different positions and orientations, but it´s necessary images overlap of the region of interest (CHENG; MATSUOKA, 2021).

Single image metric information extraction (monocular restitution) was proposed by Makarovik (1973). According to Mitishita (1997), this procedure enables planimetric mapping. The lack of stereoscopic vision is compensated with external altimetric data, for example, by a digital elevation model or a point cloud obtained by Laser scanner Technologies. Despite some advantages, like low-cost digital mapping and operation facilities, monocular restitution had few practical applications given its disadvantages, especially the computational limitations, from the low processing and storage capacity (SOUZA; CENTENO, 2014).

The most rigorous mathematic model considering the projective geometry in image acquisition used in Photogrammetry is based on the collinearity condition between a point (P) placed on the physical surface, the perspective center or exposure station from the lens system (CP), and the homologous surface point observed on the image (p') (MIKHAIL; BETHEL; MCGLONE, 2001).

However, in practical terms, the collinearity condition does not occur due to the influence of systematic errors, such as lens distortions, photogrammetric refractions, and sensor-related deformations, which affect the propagation of the light ray, displacing the image point (MITISHITA, 1997). Some of these errors are parameterized through the camera calibration process, which allows determining interior orientation parameters (IOP) (YUSOFF et al., 2017). In this approach, should be considered the determination of the exterior orientation parameters (EOP) that characterize the position (X0,Y0, Z0), and orientation in terms of attitude (, ,) of photogrammetric camera at the moment of image acquisition (KIRCHHÖFER et al., 2012).

Collinearity condition-based modeling still requires image space transformations aiming to convert image coordinates to the photogrammetric referential system (WOLTER, 2000). On this referential, IOP and EOP enable the reestablishment of the projective geometry of the image acquisition (MITISHITA; SARAIVA; MACHADO, 2003). In the case of digital images, the points measurements in the image are referenced in the digital image referential (Pixel referential: rows, columns), three transformations are necessary: 1) Pixel referential to the image millimeter frame; 2) Image millimeter frame to the photogrammetric referential with distortions; 3) photogrammetric referential with distortions to the photogrammetric referential without distortions.

According to Debiasi, Sousa e Mitishita (2011), generalized mathematic models may be used in metric information extraction. These models do not describe physically the image acquisition geometry, however, they may be considered as simplified solutions. Among these models, the Direct Linear Transformation (DLT), which is a generalized model developed by Abdel-Aziz; Karara (1971). This transformation is a combination of the General Affine two-dimensional transformation with the collinearity equations (ABREU; ANTUNES, 2017).

The last decades were marked by significant computational developments that provided cheaper equipment, consequently, the development of low-cost acquisition systems that continue to contributes to the automation and improvement of processes in different areas of knowledge. In Photogrammetry, computational applications currently go beyond the traditional demand for cartographic data, as in the railway industries (SONI et al., 2015), oil company (HOU et al., 2014) and equipment (GRANSHAW et al., 2017); cultural heritage (KIRCHHÖFER et al., 2012); anthropology and related themes such as archeology, paleontology (LUSSU; MARINI, 2020); forensic investigations (LEIPNER et al., 2019); and medicine (PIVOTTO; NAVARRO; CANDOTTI, 2021).

Also in the scope of Photogrammetry, these advances have enabled automation in obtaining altimetric information, such as through Lidar (Light Detection And Ranging, systems that use laser to determine three-dimensional point coordinates), enabled the extraction of cartographic information with the monocular restitution. In the same context, the advent of systems related to Remotely Piloted Aircraft (RPA) has reduced operating costs and bring numerous advantages over conventional photogrammetric methods. According to Lobo et al. (2020), the RPA comprises the Unmanned Aerial Vehicles (UAV), generically known as Drones, with a number exceeding 75 thousand RPA registered in the National Civil Aviation Agency of Brazil, of which 62% for the professional activities. However, for cases in which low-cost sensors are used, which involves a large part of RPA systems, the estimation of calibration parameters and sensor position and orientation, may still represent a limitation in terms of physical accuracy of the parameters that describe the geometry of image formation, mainly due to the breakdown of mathematical correlations between these parameters (YANAGI; CHIKATSU, 2015; ANDRADE, 1998). Furthermore, rigorous modeling must consider the assembly parameters of the sensors that make up the photogrammetric acquisition systems. In these cases, the DLT is an alternative to physical modeling, as it makes it possible to neglect the IOP and EOP, as well as to reduce the modeling process steps.

The main advantage of DLT is the possibility of its application without prior knowledge of accurated sensor information. It allows the extraction of information even for analogic images since that at least six control points are available. This makes it possible, for example, to retrieve historical information. In terrestrial Photogrammetry, DLT is a possibility in the mapping of facades and monitoring of mass displacement (LIU; HUANG, 2016); it can also be expanded to be used in orbital images (MITISHITA; SARAIVA; MACHADO, 2003). According to El-Ashmawy (2018), the DLT can be used as an alternative in the process of camera calibration (self-calibration), because, although EOP and IOP have physical meaning, these parameters are implicitly in the DLT equations, and can be estimated through specific formulation (DEBIASI, 2008). In addition, DLT has been used in computer vision, robotics, and biomechanics (EL-ASHMAWY, 2018).

The scope of this study is to evaluate the performance of the DLT, compared to the collinearity equations, for extracting metric information from a singular image obtained by RPA.

2. Methodology

An algorithm was implemented in Matlab software (version R2015a) to extract and compare planimetric information from an image using two mathematical models: by the rigorous collinearity equations (CLN), which have physical meaning but require prerequisites; and by the generalized DLT transformation. The two approaches were compared and evaluated. Through statistical inferences and checkpoints, it was possible to estimate the modeling accuracy. Additionally, results were evaluated according to the Brazilian Cartographic Accuracy Standard (PEC-PCD).

Algorithm settings and input data are described in sections 2.1 and 2.2. In sections 2.3 and 2.4 the formulations by CLN and DLT models are presented, respectively. The results comparison and evaluation were also considered in the algorithm, except PEC-PCD evaluation, which was carried out externally. Further details are presented in section 3.

2.1. Imaging sensor

The digital image used (Figure 1) was obtained by a off-the-chelf digital camera. Table 1 shows Interior Orientation (IOP) sensor parameters obtained from the calibration certificate of the camera.

Table 1– Interior and Exterior Orientation Parameters.

Parameter	Value	Precision
f	15.889 mm	0.006 mm
x_{pp}	0.175 mm	0.004 mm
y_{pp}	-0.095 mm	0.004 mm
k_1	-2.5484828e-04 mm	4.1836555e-06 mm
k_2	1.4890137e-06 mm	2.5989988e-08 mm
k_3	0.0	0.0
P_1	-8.9210720e-05 mm	6.5845299e-06 mm
P2	-8.0052830e-05 mm	5.6423568e-06 mm

Source: The authors.

This digital camera, model Nex-3 from Sony, is a passive RBG imaging sensor in the visible spectrum. The camera solid sensor has 3344 x 2224 pixels with each pixel measuring 0.007 mm. The camera was fixed to an RPA platform. The flight height was approximately 300 meters.

2.2. Control points and Checkpoints

A set of twelve GCP local topographic referenced referenced in the 3D local geodesy frame (accuracy: σX, σY, σZ = 0.10 m) was used. The GCPs datasets were collected through a GNSS (Global Navigation Satellite System) surveying carried out in the study region; a set of 12 points, well distributed on the image, were selected as control and checkpoints.. Six points were selected as control points, the others were adopted as checkpoints, therefore, not used for modeling. It was decided to use six control points, which is equivalent to the minimum number necessary for the DLT model. As the choice of these points can influence the quality of generated products (ZANETTI, 2017), an initial selection of points considering the best spatial distribution on the image, shown in Figure 1, was performed to minimize random errors influence (points 57, 84, 94, 108, 127 and 138). Although a different set of points configurations were processed, the initial configuration was kept as it provided better results. The points nomenclature comes from the GNSS survey.

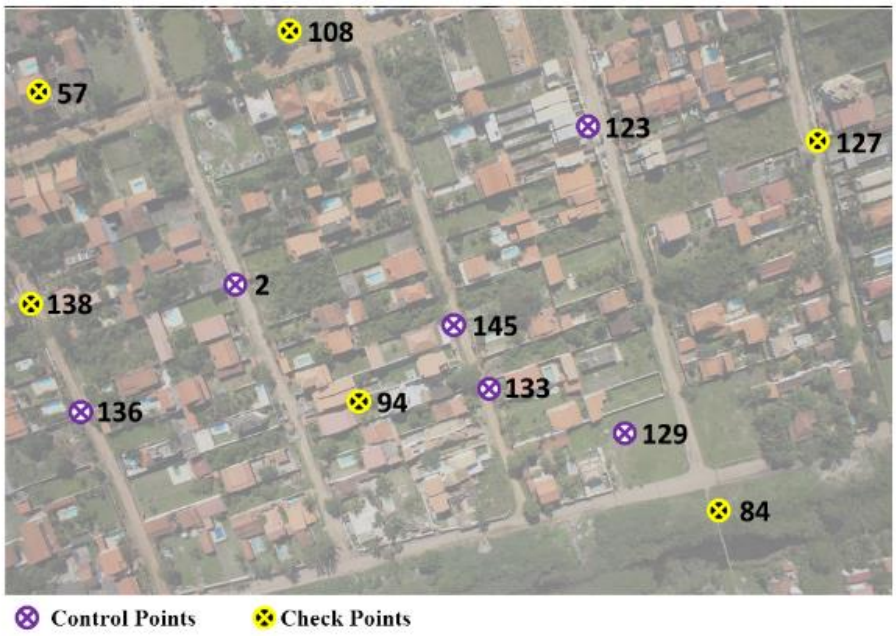

Figure 1 – Single Image – Control points (purple) and Check points (yellow).
Source: The authors.

The MultiSpec software (version 2020.02.29) was used to read the coordinates of the twelve points in the image (in pixels). 1 pixel was considered as measurement precision. Image and object space coordinates, as well sensor calibration parameters (for CLN), were used as algorithm input data.

2.3. Rigorous modeling: Collinearity Equations

Modeling by CLN was adopted to validate the results obtained with the DLT. In the following sections (2.3.1 to 2.3.5) modeling steps are presented, involving transformations between references systems (2.3.1 and 2.3.2); minimization of systematic errors related to the process (2.3.3); estimation of EOP (2.3.4); and estimation the planimetric coordinates of the checkpoints (2.3.5).

References systems transformations are necessary to the compatibility of the measurement system (digital referential) and the photogrammetric referential, to which the image coordinates must be referenced before collinearity equations application, once it is related to the image projective geometry (MITISHITA; OLIVAS, 2001).

2.3.1. Pixel Referential to Image Millimeter Frame

The twelve GCPs were measured in the pixel referential; the obtained results were column and row coordinates (c_i, l_i), in the digital reference, with *i* ranging from 1 to 12 (number of points). Normally this system is characterized by a two-dimensional Cartesian plane. The origin of the system is in the upper left corner (SCURI, 2002). On the horizontal direction from the origin, there is an increase in the number of columns to the right (0 – c axis). On the vertical direction, rotated 90º from the horizontal axis in the clockwise direction, the 0 – l axis (number of lines). Digital referential coordinates are converted to the millimeter referential (x_{mm}, y_{mm}), through Equations 1 and 2 (SANTOS, 2009):

$$x_{mm} = \frac{c - NTC - 1}{2} * Tp \quad (1)$$

$$y_{mm} = \frac{l - NTL - 1}{2} * Tp \quad (2)$$

where*: NTC*, *NTL*, *Tp* denotes the total number of columns (3344) and rows (2224) and pixel size (0.007mm).

The millimeter referential is defined by a two-dimensional Cartesian plane originating from the center of the image. The 0 - x_{mm}, axis is parallel to 0-c axis, and the 0 - y_{mm} axis is perpendicular to 0 - x_{mm}, with 90 degrees from it, featuring a right-handed system (SANTOS, 2009).

2.3.1. Image millimeter frame to the Photogrammetric Referential

The photogrammetric referential is 3D Cartesian frame in image space (x_p, y_p, z_p); its origins in the CP position. The 0 - x_p axis is coincident with the flight direction. The plane defined by $x_p y_p$ is perpendicular to the image plane. The 0 - z_p axis is coincident with the optical axis of the camera whose direction makes the system right-handed. According to Mitishita (1997), for monoscopic observations, z_p is constant and equivalent to the focal length of the camera.

The transformation between the Image referential in millimeters to photogrammetric referential consists consists in a translation (Eq. 3 and 4) that represents the mismatch between the origin of the millimeter referential and the principal point (PP), which is the intersection point of the extension of the optical axis with the image plane (SANTOS, 2009).

$$x_p = x_{mm} - x_{PP} \quad (3)$$

$$y_p = y_{mm} - y_{PP} \quad (4)$$

In these equations, x_{PP} and y_{PP} are the PP coordinates, provided by the camera calibration certificate. With this translation, the coordinates in the digital referential in mm are converted to the photogrammetric referential, obtaining coordinates in the photogrammetric referential with distortions. These coordinates still need to be corrected from distortions to minimize systematic errors that affect the condition of collinearity.

2.3.3. Transformation to photogrammetric referential without distortions

The transformation of photogrammetric referential with distortions to the photogrammetric referential without distortion is done by correcting the systematic errors that affect the condition of collinearity (MITISHITA; KIRCHNER, 2000). The mathematical formulations usually used for these corrections are given by Equations (5) and (6):

$$x'_p = x_p - \delta_r x_p - \delta_d x_p \quad (5)$$

$$y'_p = y_p - \delta_r y_p - \delta_d y_p \quad (6)$$

where x'_p and y'_p are the undistorted photogrammetric coordinates; *r* is the radial symmetric correction; *d* the decentering correction.

Except for PP, all pixels are distorted with magnitude directly related to the distance to this point. These distortions affect the theoretical condition of collinearity existing between the object point, the projection center, and the image point. In general, lens distortions are larger and commonly known as radial symmetric distortion and decentering distortion. According to Zhou et al. (2013), these distortions come from imperfections in the manufacturing process and corrections are made through parameters calculated in the calibration process (YANAGI; CHIKATSU, 2015).

In this research, according to obtained camera calibration certificate values, only these lens distortions were considered, as already mentioned, they are the most significant distortions (YUSOFF et al., 2017). Additionally, for monocular restitution applications, due to inaccuracies caused by the Digital Terrain Model (DTM) altimetry interpolations, systematic errors correction can be simplified (MITISHITA, 1997).

Regarding the image distortion due to photogrammetric or atmospheric refraction, considering different atmospheric densities through which the light ray propagates, the effect modeling cannot be performed through a simple camera calibration using a terrestrial test field; normally, a theoretical refractive index is considered (AGRAFIOTIS; GEORGOPOULOS, 2015). The refractive index, in the case of the use of the real atmosphere, is complex and requires, for example, environmental information and compositional parameters at the time of image acquisition, which was not available for this study. Furthermore, the average flight height was significantly lower when compared to conventional photogrammetric surveying. For sensor deformations modeling, it is an important procedure in Photogrammetry using analog metric cameras, being performed by the affine general 2D, projective, or polynomial transformations (WOLTER, 2000). In the current state of technology, digital camera sensors can be considered rigid, with negligible geometric distortions (MERCHANT; CASTLEMAN, 2009).

2.3.3.1. *Radial Lens Distortion*

Radial lens distortion represents the undesirable portion of refraction suffered by a light ray when passing through the objective (ANDRADE, 1998), is highly correlated to the focal length, and its modeling is given by Equations 7, 8, and 9 (YANAGI; CHIKATSU, 2015):

$$\delta_r x_p = (k_1 r^3 + k_2 r^5 + k_3 r^7) x_p \quad (7)$$

$$\delta_r y_p = (k_1 r^3 + k_2 r^5 + k_3 r^7) y_p \quad (8)$$

$$r = \sqrt{x_p^2 + y_p^2} \quad (9)$$

where: k_1, k_2 and k_3 are coefficients determined through a camera calibration process, and *r* is the Euclidean distance between a considered point and PP.

2.3.3.2. *Decentering Distortion*

This distortion comes from the impossibility of the perfect alignment of the lens's optical axis. It is composed of tangential and radial asymmetric distortions (ANDRADE, 1998). The distortion model is given by Equations 10 and 11 (LERMA; CABRELLES, 2007):

$$\delta_d x_p = P_1\ (r^2 + 2x^2)\ +\ 2P_2\ x_p y_p \qquad (10)$$

$$\delta_d y_p = P_2\ (r^2 + 2y^2)\ +\ 2P_1\ x_p y_p \qquad (11)$$

where P_1 and P_2 are determined through the camera calibration process.

2.3.4. Space Resection

Space resection refers to the image EOP determination process (GEMAL; MACHADO; WANDRESEN, 2015). Traditionally, EOP are indirectly determined using control points and the least-squares method, using collinearity equations in their direct form as a mathematical model (Eq. 12 and 13). Alternatively, EOP parameters can be directly determined at the acquisition instant, when the image sensor has a GNSS/INS integration (PEDROSA; SANTOS, 2020).

$$xp' = -f\frac{m_{11}(X - Xo) + m_{12}(Y - Yo) + m_{13}(Z - Zo)}{m_{31}(X - Xo) + m_{32}(Y - Yo) + m_{33}(Z - Zo)} \qquad (12)$$

$$yp' = -f\frac{m_{21}(X - Xo) + m_{22}(Y - Yo) + m_{23}(Z\ - Zo)}{m_{31}(X - Xo) + m_{32}(Z - Yo) + m_{33}(Z - Zo)} \qquad (13)$$

Equations 12 and 13, presents measurements (coordinates of points on photogrammetric referential without distortions) as a function of parameters; *X*, *Y*, *Z* are control point coordinates in the referential measured on the object space; the elements m_{11} to m_{33} represent rotation matrix elements which are defined by sensor attitude angles; and *f* the focal length (EL-ASHMAWY, 2015).

The indirect estimation of the EOPs can be performed by the least-squares adjustment with position constraint functions that are weighted using control points precisions. The constraint equations were added (Eq. 14). As it is a non-linear adjust, approximated parameters values were required, and definitive parameters being calculated through an iterative process. The Lest Square Adjustment was performed by Matlab software routines, using the proposal shown in Gemal, Machado, and Wandresen (2015).

$$\begin{aligned} XL(obs) - X(cal) &= 0 \\ YL(obs) - Y(cal) &= 0 \\ ZL(obs) - Z(cal) &= 0 \end{aligned} \qquad (14)$$

where: *XL*, *YL*, and *ZL* are control points coordinates measured through GNSS field surveying (observations); and *X*, *Y*, *Z* are the control points coordinates calculated by the adjustment.

2.3.5. Obtaining planimetric coordinates by CLN

The geodesic planimetric coordinates of points, measured in the image, can be performed Collinearity equation in the inverse form, shown in equations 15 and 16 (ARSLAN, 2014). The altimetric coordinates were computed by a DTM dataset (Z_{DTM}).

$$XL = Xo + (Z_{MDT} - Zo)\frac{m_{11}xp + m_{21}yp + m_{31}f}{m_{13}xp + m_{23}yp + m_{33}f} \quad (15)$$

$$YL = Yo + (Z_{MDT} - Zo)\frac{m_{21}xp + m_{22}yp + m_{32}f}{m_{13}xp + m_{23}yp + m_{33}f} \quad (16)$$

Figure 2 shows the convergence process and elements involved in the computation of planimetric coordinates using CLN inverse equations with the regular surface defined by a DTM, making it possible to convert coordinates from the photogrammetric referential to the local geodesy referential.

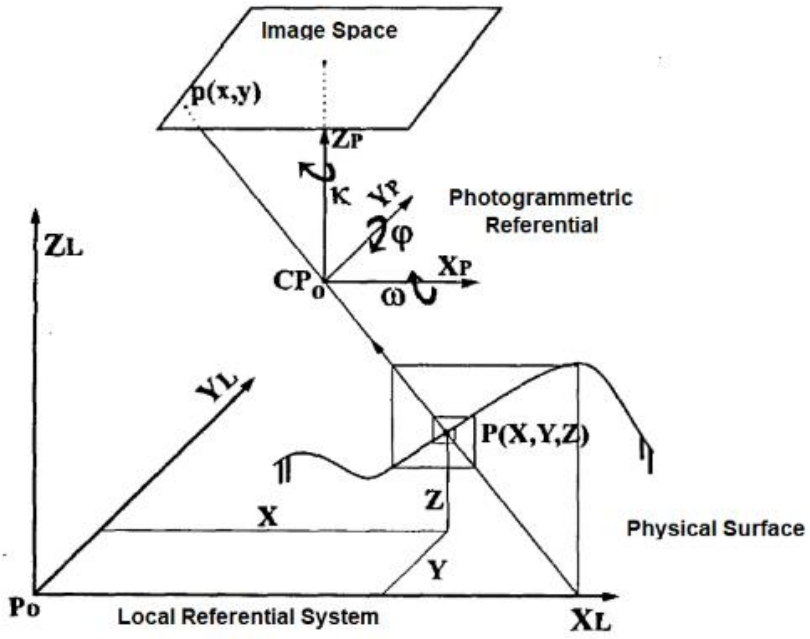

Figure 2 – Iterative convergence process for obtaining horizontal information using a single image through CLN. Source: Mitishita (1997).

2.4. Generalized Modeling: Direct Linear Transformation

Through the DLT, it is possible to carry out the direct linear relationship between digital referential coordinates and object referential space coordinates, as indicated in equations 17 and 18 (DIAS; MITISHITA; DALMOLIN, 2012), therefore, it reduces steps concerning collinearity. In addition, it makes it possible to estimate 2D and 3D information through specific formulations (SOUZA; CENTENO, 2014).

$$c = \frac{L_1X + L_2Y + L_3Z + L_4}{L_9X + L_{10}Y + L_{11}Z + 1} \quad (17)$$

$$l = \frac{L_5X + L_6Y + L_7Z + L_8}{L_9X + L_{10}Y + L_{11}Z + 1} \quad (18)$$

where *c*, *l* are digital referential coordinates; *X, Y, Z* object space referenced coordinates; and L_1 to L_{11} DLT parameters.

The six control points, used to model the CLN inverse equations, were considered for this application. According to equations 17 and 18. Each point measured in the image referential provides two measurements (c, l), two equations per point. The 11 unknown parameters equation system resolution implies a larger number of equations. With six control points, 12 equations are available, therefore, it makes system solution via least-squares adjustment possible.

The use of DLT for planimetric information extraction requires parameters determination through equations in the direct form (Eq. 17 and 18) having measurements of the control points in the image space and the object space (EL-ASHMAWY, 2018). Subsequently, by inverse DLT form, the planimetric coordinates of the points in the object space can be obtained using the 11 parameters previously calculated, image points measurements, and altimetric coordinate (Z) computed by a DTM, according to the approach presented by Equations 19, 20, 21 (MITISHITA; SARAIVA; MACHADO, 2003):

$$[X\ Y\ ] = A^{-1}C \quad (19)$$

$$A = [L_1 - cL_9\ L_2 - cL_{10}\ L_5 - cL_9\ L_9 - L_{10}\ ] \quad (20)$$

$$C = [-Z(L_3 - cL_{11}) - L_4 + c\ -Z(L_7 - lL_{11}) - L_8 + l\ ] \quad (21)$$

3. Results and discussion

Each model performance was initially evaluated, verifying the least-squares adjustment accuracy performed on parameters determination. The results accuracy was verified by comparing the coordinates calculated by the CNL and DLT against the checkpoints reference coordinates. The Brazilian Cartographic Accuracy standard of the planimetric coordinates was evaluated.

3.1. Modeling evaluation

Table 2 presents the parameters by CLN (EOP). These results were obtained by the Space Resection, presented in section 2.3.4, after six iterations. Table 3 shows the residuals (in millimeters) obtained in the adjustment to determine the parameters of the CLN.

Table 2 – Parameters obtained in rigorous modeling.

Parameter	Value	Precision
X_0 (m)	587.885	0.450
Y_0 (m)	547.327	0.551
Z_0 (m)	292.472	0.128
ω (rad)	- 0.096	0.002
φ (rad)	0.016	0.001
κ (rad)	- 0.369	0.0005

Source: The authors.

Table 3 – Adjusted residual through CLN.

Control Point	vX (mm)	vY (mm)
57	-0.0015	0.0084
84	0.0068	-0.0061
94	0.0054	0.0015
108	-0.0053	-0.0009
127	-0.0081	-0.0048
138	0.0146	0.0007

Source: The authors.

When performing an analysis of the residuals in the adjustment (v) presented in Table 3, it is verified that values obtained are predominantly within the range defined by the adopted precision for the measurements (0.007 mm, corresponding to the dimension of a pixel). However, three measurements showed residuals out of the expected: in the measurement of the X component of point 138 (0.0146 mm, this being the largest residue obtained); in the X component of point 127 and the Y component of point 57. It is noteworthy that the unit, in this case, is in millimeters, since this is the unit of measurements (photogrammetric referential points coordinates) that make up the vector of observations.

A statistical test (χ^2) was applied to assess adjustment and parameters accuracy obtained. However, it is noteworthy that the adjustment precision obtained does not guarantee the process's accuracy. For the statistical test, the *posteriori* variance calculation ($\hat{\sigma}_0^2$) was performed by Equation 22. This value indicates its consistency as an unbiased estimator of the a priori variance (GEMAL; MACHADO; WANDRESEN, 2015).

$$\hat{\sigma}_0^2 = \frac{V^T P V}{n - u} \tag{22}$$

where: V is the residuals vector; P is the Weights Matrix; n the number of equations; and u indicates the number of unknowns. However, as a least-squares adjustment by weighted constraint method was used, this equation is modified (Equation 23):

$$\hat{\sigma}_0^2 = \frac{V^T P V + E^T P_C E}{n - u} \tag{23}$$

where E is the closing error injunctions vector; and P_C is the weight control points matrix.

The denominator of equations 22 and 23 refers to degrees of freedom. In this modelimg there are 24 degrees of freedom since n = 30 equations were obtained, being 12 equations (two equations per point, having six control points); and 18 injunction equations. On the other hand, u = 6 unknown parameters (EOP).

The *posteriori* variance calculated was 1.0956. It is verified that the *posteriori* variance had a value very close to the *prior*i variance ($\sigma_0^2 = 1$) indicating that the measured residuals, obtained from adjustment, present values close to the adopted variances for the measures or the weights (accuracies) assigned to the measures were adequate. In the hypothesis test (χ^2), the χ^2 was calculated according to Equation 24, obtaining the value of 26.2949.

$$\chi^2 = \hat{\sigma}_0^2 * (n - u) \tag{24}$$

The ranging limits for accepting the null hypothesis was 12,401 = $\chi^2_{2.5\%} < \chi^2 > \chi^2_{97.5\%}$ = 39,364, therefore, the null hypothesis was accepted. In practice, this result indicates the mathematical model used validity and the absence of gross errors and that the system is well-conditioned.

In the DLT modeling, 11 parameters were estimated (Table 4). The solution convergence was achieved after seven iterations. Unlike collinearity, these parameters do not have a direct physical meaning. Furthermore, each of these eleven parameters represents a specific mathematical formulation. Therefore, the comparison between parameter values is not feasible. Table 5 shows the adjustment residuals (in pixels) for the parameters determined through DLT modeling.

Considering the adjustment residuals analysis, it is verified that the obtained values are within an interval defined by the adopted precision of measurement (1 pixel). The biggest residual (v) are related to the *X* and *Y* component of point 94, with vx = 0.39 pixel and vy = -0.41 pixel. In the hypothesis test, the χ^2 obtained was 0.5651, corresponding to the same *posteriori* variance value, since we have one degree of freedom, as 11 unknown parameters were modeled by the DLT equations with 12 equations.

The range limits for accepting the null hypothesis were $0.001 = \chi^2_{2.5\%} < \chi^2 > \chi^2_{97.5\%} = 5.024$, therefore, as in the collinearity modeling, the null hypothesis was accepted, indicating the mathematical model used validity.

Table 4 – Parameters obtained in DLT modeling.

Parameter	Value	Precision
L_1	6.1824	0.0440
L_2	-2.5819	0.0097
L_3	-5.2736	0.1607
L_4	-807.0954	12.5376
L_5	-2.2018	0.0149
L_6	-6.45295	0.0353
L_7	-3.1803	0.1845
L_8	5605.471	33.9426
L_9	-0.00003	0.000002
L_{10}	-0.00023	0.00002
L_{11}	-0.00391	0.0004

Source: The authors.

Table 5 – Adjustment residuals DLT.

Control Point	vx (pixels)	vy (pixels)
57	-0.0646	0.0697
84	-0.2132	0.3352
94	0.3898	-0.4077
108	0.014	0.1643
127	0.0185	-0.1772
138	-0.1444	0.0156

Souce: The authors.

Through the analysis of the adjustments, it was found that the modeling performed by the DLT presented better performance than that obtained by the collinearity equations, which may be related to the greater suitability of the DLT, which is a generalized model; thus, the collinearity equations, which have a physical meaning, are more rigorous, and in this case, inaccuracies in the IOPs or the non-correction of the distortion, related to the photogrammetric refraction, may be contributed to the results obtained with the collinearity equations.

3.2. Discrepancies assessment

To verify the CLN and DLT model's accuracy through the monocular restitution, six checkpoints were used. The planimetric coordinates (*Xi* and *Yi*) of the checkpoints were calculated using equations 15 and 16 for the CLN model and equations 19, 20, and 21 for the DLT. The altimetric coordinates (*Zi*) of the checkpoints were used in CLN modeling. The discrepancies values were obtained using equations 25, with i ranging from 1 to 6.

$$dXi = XLi - Xi$$
$$dYi = YLi - Yi \quad (25)$$

The discrepancies by CLN are shown in Table 6. The biggest discrepancy is obtained at point 129, in the Y component (0.80 m). The average discrepancy in the X component was -0.2367 m, with a standard deviation of 0.2620 m and root mean square error (RMSE) of 0.34 m. For the Y component, the average discrepancy was 0.3298 m, with a standard deviation of 0.2589 m and RMSE of 0.41 m. Additionally, the planimetric discrepancies were evaluated, considering the combination os discrepancies in X and Y components. The mean planimetric discrepancy for collinearity was 0.41 m, with RMSE 0.53 m.

Table 6 – CLN Differences.

Point	dX (m)	dY (m)
002	-0.0705	0.1093
123	-0.0544	0.2910
129	-0.7374	0.8057
133	-0.3118	0.4126
136	-0.1153	0.2386
145	-0.1305	0.1216

Source: The authors.

By the Figure 3, it can be seen that the discrepancies in X (Dx) had a similar behavior for all points (all negative values), in turn, in the Y direction (Dy) they were positive. Note that point 129 is the point with the highest values, the planimetric discrepancy (EP) at this point was bigger than 1 m.

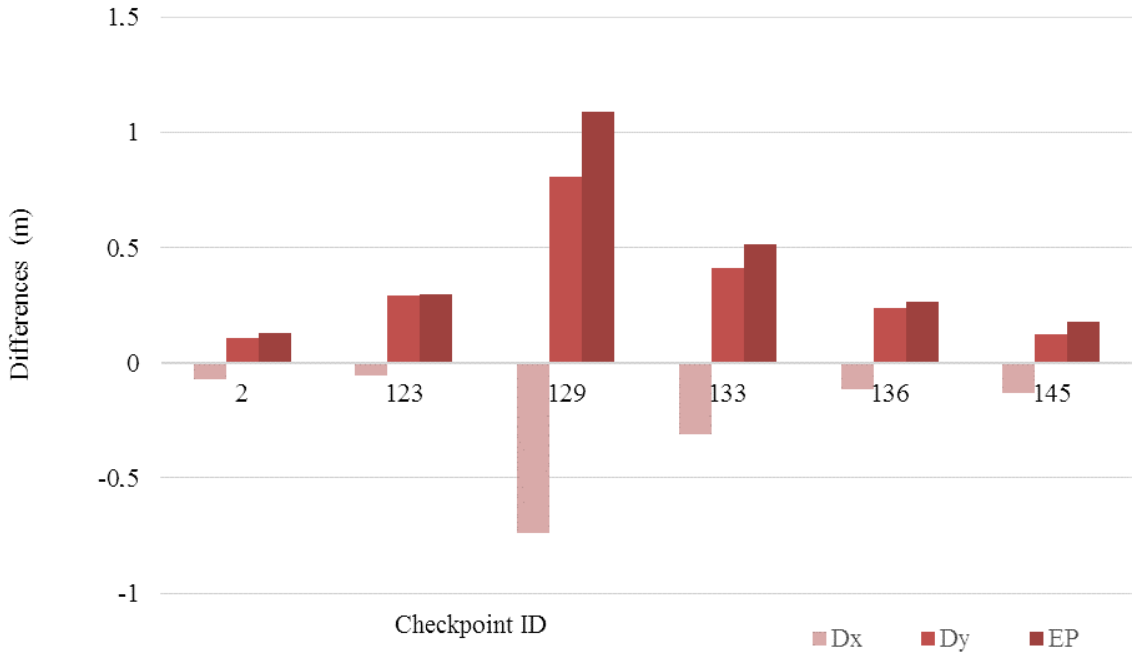

Figure 3 – Discrepancies between references coordinates obtained against CLN
Source: The authors.

Through DLT, the biggest discrepancy between the components did not occur at point 129 (Table 7) like in the CLN model. The largest discrepancies occurred at point 136 in at X component, and point 133, in Y component.

In calculating the discrepancy average, the value of 0.3655 m was obtained, with a standard deviation of 0.2619 m in the X component and RMSE of 0.44 m. For the Y component, the average discrepancy was -0.1976 m, with a standard deviation of 0.3374 m and RMSE of 0.37 m. In planimetric discrepancies, the average was 0.52 m, with RMSE 0.57 m. In Figure 4 the differences between the reference coordinates and those obtained by the DLT are presented.

By analyzing Figures 3 and 4, the differences obtained through DLT and CLN can be verified. Lower planimetric accuracy was expected with the DLT model, as this model is generalized and its parameters are mathematical without physical meaning. In both models, the biggest differences are in the order of decimeters.

Compared to the results obtained with the modeling through CLN, it appears that the DLT showed a significant proximity to these results, obtaining an average planimetric error difference of 10 cm, therefore, in the same order of magnitude as the control points precision used to the modeling. Based on the RMSE planimetric differences results, the DLT showed approximately 90% efficiency compared to the rigorous formulation.

Table 7 – Differences through DLT.

Point	***dX* (m)**	***dY* (m)**
002	0.1335	-0.0048
123	0.1237	0.3380
129	0.4053	-0.5060
133	0.3458	-0.5815
136	0.8432	-0.1841
145	0.3413	-0.2475

Source: The authors.

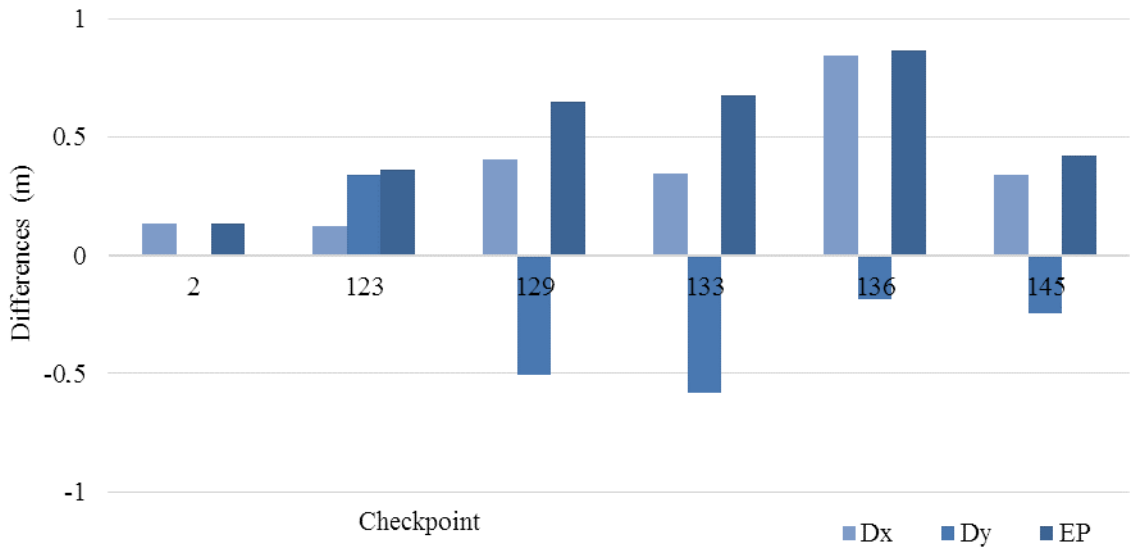

Figure 4 – Differences between reference coordinates and obtained through DLT.
Source: The authors.

In Figure 5, the arrows represent the planimetric discrepancies vectors between the coordinates obtained by the CLN and the DLT in relation to the reference coordinates of the checkpoints in the local topographic system. The bars around the reference points indicate the precision of the coordinates. A scale factor was applied to the figure elements to facilitate the quantities visualization. These vectors indicate the spatial distribution, magnitude, and direction of the discrepancies. From these results, an investigation was carried out to assess possible trends in the modeling (section 3.2.1).

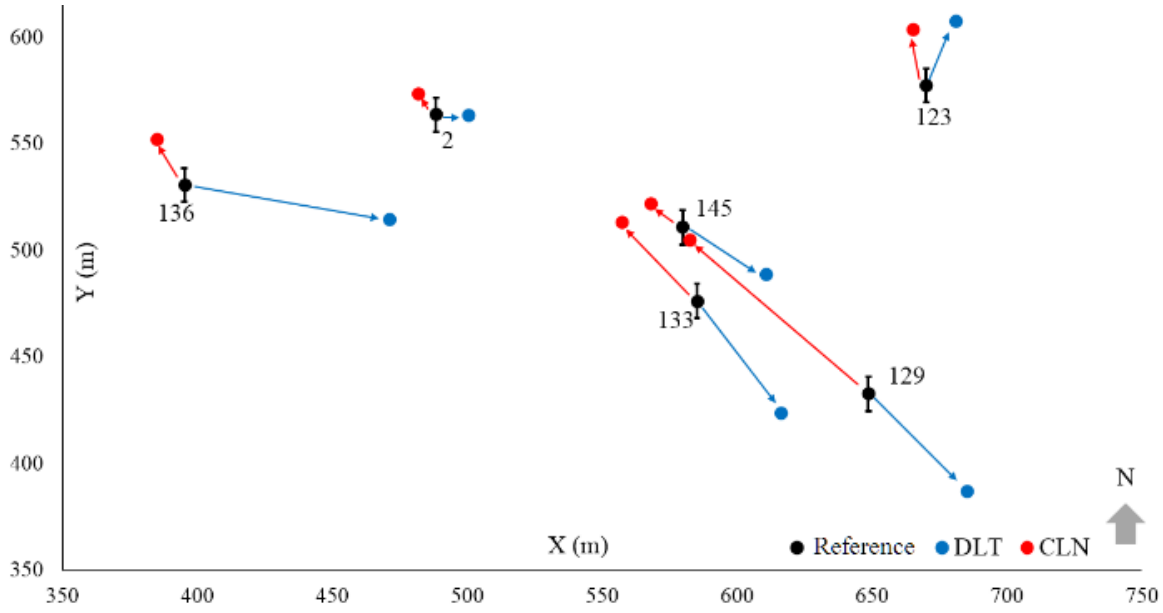

Figure 5 – Planimetric diferences indicative vectors.
Source: The authors.

3.2.1. Trend Assestment

In this evaluation, it was considered that the average discrepancies statistically equal to zero, within a certain level of significance, admit the non-existence of trends in results (GALO; DAL POZ; FERREIRA, 2001). Statistical Student *t*-test was used. It is calculated through the equation presented in 26, according to Galo, Dal Poz, and Ferreira (2001):

$$t_X = \frac{\Delta\bar{X}}{s\Delta X} * \sqrt[2]{n} \qquad (26)$$

where: $\Delta\bar{X}$ is the X component discrepancies average; $s\Delta X$ is the standard deviation of the discrepancies; and *n* indicates the sample size, in this case the number of checkpoints. The acceptance condition (trend-free modeling) is indicated in equation 27, in which the value of *t* is tabulated and depends on the sample size and confidence interval.

$$|t_X| < t_{\left(n-1,\frac{\alpha}{2}\right)} \qquad (27)$$

Adopting 90% of confidence interval, t = 1.440 was defined. For Collinearity, t_X= -2.2127 and t_Y= 3.1204 were obtained, therefore, the initial hypothesis is rejected, indicating that there is a tendency towards the X component and also towards Y. According to Galo and Camargo (1994), the trend existence in any direction indicates the occurrence of some inconsistency that may have different causes. By DLT, the values obtained were t_X= 3.4180 and t_Y= -1.4349, indicating that there is a trend towards the X component.

These values complement the graphic results shown in Figure 5, in which it can be seen that all points calculated by collinearity have a displacement in relation to the reference points in approximately the same direction (Northwest), with azimuths of approx. of 315°. A small variation of this direction is seen at point 123. Concerning DLT, it appears that most of the vectors have approximately the same direction as for collinearity, but in opposite directions (Southeast), with emphasis on points 129, 133 and 145, which are located in the same region of the image. The direction with the higher discrepancy also occurs as in collinearity, at point 123.

The combined analysis of the trend test and Figure 5 corroborates the hypothesis of trend in the results, which may indicate the influence of some systematic error in the process modeling, which may be related to image acquisition, modeling equations, or even the determination of control points. In this sense, it is noteworthy that in the modeling, the processing was carried out using different configurations of the 12 points, and the best results achieved are presented here.

3.2.2. Brazilian Cartographic Accuracy Standard Evaluation

To complement the analyses, the Cartographic Accuracy Standard for Digital Cartographic Products (PEC-PCD) established by Geographical Service of the Brazilian Army (DSG) in the National Spatial Data Infrastructure-INDE (DSG, 2011) was calculated, considering the product suitable in class A by CLN and class B by DLT, on a scale of 1:10,000.

4. Final considerations

In this work, a comparison of planimetric information obtained by DLT and CLN modeling was performed using an image collected with RPA. Based on the results, it was verified that both models allowed to estimate the planimetric coordinates with significant accuracy. Mean discrepancies were less than 0.30 m for CLN and less than 0.40 m for DLT. As expected, the results are less accurate than expected with the combined use of two or more images, but allow acceptable results when at least one stereo-pair is not available. The disadvantage of mono-restitution is the need for altimetric data from external sources.

In strategies carried out to obtain the best configuration of control/check points, it was found that the discrepancy results worsened depending on the selection of checkpoints, mainly by the CLN, requiring a more careful selection of control points. In modeling, the resulting parameters remained constant for several configurations of control points tested, even for points not considered ideal, such as the edge of roofs.

More accurate results could be obtained with the CLN model, if the camera was calibrated at work, enabling a better deviations modeling from the collinearity condition, such as those caused by photogrammetric refraction. In this sense, mono-restitution experiments, involving on-the-job calibration, are recommended.

The good performance of the DLT stands out, since it provided results comparable to those obtained with the collinearity equations with 90% efficiency, having the advantages such as relative facilities of operation and independence of sensor parameters. Despite this, the results suggest the possible occurrence of systematic errors in the process. For future investigations: the possible influence of these errors on the extraction of metric information from an image; the technique validation through replicability to other areas; and comparison with methods that employ the use of two or more images.

The algorithm implementation allowed process control, which not always occurs with commercial software. In future works, the algorithm can be extended to consider the use of a stereo-pair and even a block of images, aiming to expand the investigations. In addition, it is intended to make it available in an institutional repository, so that it can be used for academic purposes.

Acknowledgements

The first and third authors thank CAPES (Coordination for the Improvement of Higher Education Personnel), for promoting the scholarships, on processes 88882.382285/2019-01 and 88887.499364/2020-00, respectively. The authors thank Professor Fabiano Freiman from the Federal University of Bahia for his valuable contributions in carrying out this paper.

References

ABDEL-AZIZ, Y. I.; KARARA, H. M. *Direct linear transformation from comparator coordinates into object space coordinates in close-range photogrammetry* In:. American Society of Photogrammetry Symposium on close-range Photogrametry - Anais. Urbana, 1971

ABREU, F. C. S.; Antunes, A. F. Monorrestituição de imagem de alta resolução Quickbird II apoiado no M.D.E. obtido com dados do sistema Laser Scanner. *Revista Tecnologia e Ambiente*, v. 23, p. 1–15, 2017.

AGRAFIOTIS, P.; GEORGOPOULOS, A. *Camera constant in the case of two media photogrammetry*. In: International Archives of the Photogrammetry, Remote Sensing and Spatial Information Sciences - ISPRS Archives, v. 40, n. 5W5, p. 1–6, 2015.

ANDRADE, J. B. *Fotogrametria*. Curitiba: Universidade Federal do Paraná, 1998. 196p.

ARSLAN, O. 3d Object Reconstruction from a Single Image. *International Journal of Environment and Geoinformatics*, v. 1, n. 1, p. 21–28, 2014.

AWANGE, J. L.; KYALO KIEMA, J. B. *Environmental Geoinformatics*. Berlin, Heidelberg: Springer, 2013. 541p.

CHENG, M.-L.; MATSUOKA, M. Extracting three-dimensional (3D) spatial information from sequential oblique unmanned aerial system (UAS) imagery for digital surface modeling. *International Journal of Remote Sensing*, v. 42, n. 5, p. 1643–1663, 2021.

COELHO, L.; BRITO, J. N. *Fotogrametria Digital*. 2. ed. Rio de Janeiro, RJ: EdUERJ, 2007. 196p.

DEBIASI, P. *Ortorretificação de Imagens CCD CBERS 2 Através da Transformação DLT*, 2008. 71f. Dissertação (Mestrado). Programa de Pós-Graduação em Sensoriamento Remoto, Universidade Federal do Rio Grande do Sul, Porto Alegre, 2008.

DEBIASI, P.; SOUZA, S. DE; MITISHITA, E. *Pesquisas em Geociências*, v. 38, n. 1, p. 55–65, 2011.

DIAS, S. O.; MITISHITA, E. A.; DALMOLIN, Q. Orientação Exterior de um par Estereoscópico Ikonos II com base no Modelo Não Rigoroso DLT. *Boletim de Ciências Geodésicas*, v. 18, n. 1, p. 40–62, 2012.

DSG. Diretoria de Serviço Geográfico. *Especificação Técnica para a Aquisição de Dados Geoespaciais Vetoriais (ET_ADGV)* Brasília, DF: DSG, 2011.

EL-ASHMAWY, K. L. A. A comparison study between collinearity condition, coplanarity condition, and direct linear transformation (DLT) method for camera exterior orientation parameters determination. *Geodesy and Cartography*, v. 41, n. 2, p. 66–73, 2015.

EL-ASHMAWY, K. L. A. Using direct linear transformation (DLT) method for aerial photogrammetry applications. *Geodesy and Cartography*, v. 44, n. 3, p. 71–79, 2018.

GALO, M.; DAL POZ, A. P.; FERREIRA, F. M. O Uso De Feições No Controle De Qualidade Em Cartografia. XIX Congresso Brasileiro de Cartografia. Anais...Porto Alegre - RS: 2001

GEMAL, C.; MACHADO, A. M. L.; WANDRESEN, R. *Introdução ao Ajustamento de Observações*. 2. ed. Curitiba: Editora UFPR, 2015. 430p.

GHILANI, C. D.; WOLF, P. R. *Elementary surveying: an introduction to geomatics*. 12. ed. New Jersey, USA: Pearson Prentice Hall, 2008. 931p.

GRANSHAW, S. I. et al. Photogrammetry and Industry. *Photogrammetric Record*, v. 32, n. 158, p. 74–92, 2017.

HOU, L. et al. *Combining photogrammetry and augmented reality towards an integrated facility management system for the oil industry*. Proceedings of the IEEE, v. 102, n. 2, p. 204–220, 2014.

KIRCHHÖFER, M. K. et al. Direct Exterior Orientation Determination for a Low-Cost Heritage Recording System. *Photogrammetric Record*, v. 27, n. 140, p. 443–461, 2012.

LEIPNER, A. et al. 3D mug shot—3D head models from photogrammetry for forensic identification. *Forensic Science International*, v. 300, p. 6–12, 2019.

LERMA, J. L.; Cabrelles, M. A review and analyses of plumb-line. *The Photogrammetric Record*, v. 22, p. 135–150, 2007.

LIU, W. C.; HUANG, W. C. Close range digital photogrammetry applied to topography and landslide measurements. International Archives of the Photogrammetry, Remote Sensing and Spatial Information Sciences - ISPRS Archives, v. 41, n. July, p. 875–880, 2016.

LOBO, F. et al. Uso de Plataformas Aéreas Não Tripuladas no Brasil – um Panorama de Dez Anos (2008-2018) de Publicações Acadêmicas. *Revista Brasileira de Cartografia*, v. 72, p. 785–806, 2020.

LUSSU, P.; MARINI, E. Ultra close-range digital photogrammetry in skeletal anthropology: A systematic review. *PLoS ONE*, v. 15, n. 4, p. 1–30, 2020.

MAKAROVIK, B. Digital Mono-Ploters. *I.T.C. Journal*, v. 1, p. 101–122, 1973.

MERCHANT, F. A.; CASTLEMAN, K. R. Computer-Assisted Microscopy. In: BOVIK, A. (Ed.). The Essential Guide to Image Processing. Boston: Academic Press, 2009. p. 777–831.

MIKHAIL, E. M.; BETHEL, J. S.; MCGLONE, J. C. *Introduction to Modern Photogrammetry*. 1. ed. [s.l.]: Wiley, 2001. 496p.

MITISHITA, E. A. *Monorestituição Digital de Aerofotos Associada com Sistema de Computação Gráfica C.A.D. para fins de Mapeamento na Área Florestal.* 278f. Tese (Doutorado). Programa de Pós-Graduação em Engenharia Florestal, Universidade Federal do Paraná, Curitiba, 1997.

MITISHITA, E. A.; KIRCHNER, F. F. Digital mono-differential restitution of airphotos applied to planimetric mapping. International Archives of Photogrammetry and Remote Sensing. Anais...Amsterdam: 2000

MITISHITA, E. A.; OLIVAS, M. A. A. Viabilidade da utilização da monorestituição na construção de base cartográfica digital urbana. *Boletim de Ciências Geodésicas*, v. 7, n. 2, p. 23–40, 2001.

MITISHITA, E. A.; SARAIVA, C. C. S.; MACHADO, Á. L. Monorestituição de imagens do satélite de alta resolução Ikonos 2 (geo), utilizando-se da transformação DLT e modelo digital de terreno. Anais do XI Simpósio Brasileiro de Sensoriamento Remoto - Belo Horizonte. Anais...Belo Horizonte: 2003

PEDROSA, J. R. B.; SANTOS, D. R. dos. Determinação dos Parâmetros de Desalinhamento Angular Usando uma Abordagem Ponto-a-Plano com Apoio de Campo Derivado de uma Nuvem LiDAR. *Revista Brasileira de Cartografia*, v. 72, n. 3, p. 460–473, 2020.

PIVOTTO, L. R.; NAVARRO, I. J. R. L.; CANDOTTI, C. T. Radiography and photogrammetry-based methods of assessing cervical spine posture in the sagittal plane: A systematic review with meta-analysis. *Gait and Posture*, v. 84, 2020, p. 357–367, 2021.

SANTOS, D. R. dos. *Elementos de Fotogrametria e Sensoriamento Remoto*. 1. ed. Curitiba: Universidade Federal do Paraná, 2009.

SCURI, A. E. *Fundamentos da Imagem Digital*. Rio de Janeiro, RJ: Pontifícia Universidade Católica do Rio de Janeiro, 2002. 67p.

SONI, A.; ROBSON, S.; GLEESON, B. Structural monitoring for the rail industry using conventional survey, laser scanning and photogrammetry. *Applied Geomatics*, v. 7, n. 2, p. 123–138, 2015.

SOUZA, G. V. DE; CENTENO, J. A. da S. Fototriangulação do triplet de imagem ALOS através da Transformação Linear Direta. Revista Ciência e Tecnologia, v. 17, n. 30, p. 1–13, 2014.

WOLTER, F. R. *Uso da Monorestituiçao Digital e DTM para mapeamento de unidades fisiográficas para estudos de solos.* 110f. Dissertação (Mestrado) Programa de Pós Graduação em Ciências Geodésicas, Universidade Federal do Paraná, Curitiba, 2000 .

YANAGI, H.; CHIKATSU, H. Camera Calibration in 3D Modelling for Uav Application. International Archives of the Photogrammetry, Remote Sensing and Spatial Information Sciences - ISPRS Archives, v. 40, n. 4W5, p. 223–226, 2015.

YUSOFF, A. R. et al. Camera calibration accuracy at different UAV flying heights. International Archives of the Photogrammetry, Remote Sensing and Spatial Information Sciences - ISPRS Archives, v. 42, n. 2W3, p. 595–600, 2017.

ZANETTI, J. *Influência do número e distribuição de pontos de controle em ortofotos geradas a partir de um levantamento por VANT*. 96f. Dissertação (Mestrado).Programa de Pós-Graduação em Engenharia Civil, Universidade Federal de Viçosa, Viçosa, 2017.

ZHOU, F. et al. Distortion correction using a single image based on projective invariability and separate model. *Optik*, v. 124, n. 17, p. 3125–3130, 2013.